

Your title
in two rows
or more

Master Thesis of

Your Name

At the Department of Physics
Institut für experimentelle Teilchenphysik
(ETP)

Reviewer: Prof. Dr. Wim de Boer
Second reviewer: Prof. Dr. Second Advisor

Duration: 1. March 2017 – 28. February 2018

I declare that I have developed and written the enclosed thesis completely by myself,
and have not used sources or means without declaration in the text.

Karlsruhe, 19th January 2018

.....
(Your Name)

Contents

1. Method	1
1.1. Data origin	1
1.2. Model components	3
1.2.1. Basic components	3
1.2.2. Additional components	4
1.3. Fitting method	6
Bibliography	9
Appendix	13
A. Some appendix section	13

1. Method

1.1. Data origin

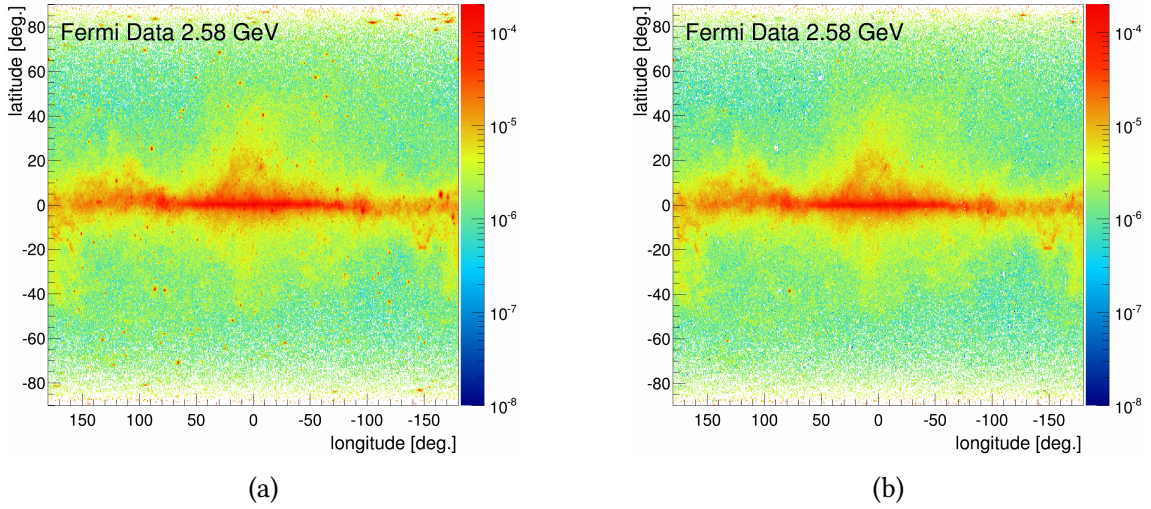


Figure 1.1.: Measured gamma ray flux before (left) and after (right) point source subtraction in $GeV/s/m^2/sr$. Most of the spots formed by point sources have disappeared, leaving only the diffuse background emission. The subtraction is not perfect, and can create artificial "holes" in the map (for example at coordinates (90, 25) or (50, 60)).

All the following work is based on the measurement of gamma rays coming from the intra- and extra-galactic sources. The quality and accuracy of the data is one of the most important point that will determine the general quality of the results. Thus it is capital to be certain that the gathering and treatment was done properly.

The Fermi collaboration Large Area Telescope (LAT) observed the gamma-ray sky since 2008 and provides all the data of this work. All the information and data are available on the web and anybody can access them, using the tools given by Fermi.

Since the observation is still on-going it is important to stay up-to-date. The treatment method is also being improved regularly, improving every time the statistics, the systematic errors and the point source subtraction. One of the most important step in the treatment process is the first one, the selection of the events. Every photon measured is saved along with all its properties in a big data file. Then this long list is filtered to keep only the interesting observations. The filter can be based on the incoming direction, the energy or the time of observation, but also on the quality of the event reconstruction. This last cut can be critical. It will determine the chances that the measured event is in fact a gamma ray, and not some background noise polluting the data. Of course, the more strict the filter is, the less events are kept for analysis and the statistical errors can become large. This work uses the CLEAN class recommended by the Fermi team for diffuse emission analysis.

The main parameters of the selection can be found in Tab 1.1.

Parameter name	Parameter value	Description
Event class	256 (CLEAN)	Quality parameter. Varies the level of background noise.
Event type	3	Back+front event.
Time boundaries	INDEF	Selecting all events since beginning of observation
Minimum energy (MeV)	58.4731	Minimum energy of the event.
Maximum energy (MeV)	513056	Maximum energy of the event.
zmax (degrees)	90	Maximum zenith angle to get rid of the Earth limb contaminations, as recommended by the LAT instrument team

Table 1.1.: List of the main parameters used for data selection.

An other important point is the creation of the exposure map. It basically tells how long the telescope spend observing a given part of the sky. After dividing the count map by the exposure, a flux map is obtained that does not depends on the observation time of particular regions.

The goal of this work is to study the diffuse sources of gamma-rays from inside and outside the milky way. Of course, the LAT does not differentiate them from point sources gamma rays. This has to be done manually as the last step in the treatment process. A large catalog of gamma ray point sources (3FGL) is available on line on NASA website. This catalog lists most of the known and identified point sources, along with their spectral shape and flux. These informations can then be used, combined with the exposure map, to model the number of counts coming from point sources and their spatial and energetic distribution. Once this model map is obtained, it is subtracted from the data to only keep the diffuse emission. Since the models are never perfect and all point sources are not listed, errors or anomalies in the observations can appear. Keeping the dataset up-to-date allows to use the latest catalogs and avoid a lot of mistakes.

Once all the treatment is done, a flux map of the entire sky in $\text{counts/s/m}^2/\text{GeV/sr}$ is produced. The map is divided in bins of 0.5×0.5 degrees on a Cartesian projection. Every bin contains 30 logarithmic energy bins ranging from 60 MeV to 513 GeV with a 1.2 multiplicative step. The final data cube is thus of dimension $720 \times 360 \times 30$. For

visibility purposes, every energy bin is multiplied by its energy squared, becoming an energy flux in $GeV/s/m^2/sr$. This will be the default units used for the rest of this work.

The errors on the data are coming from two sources. First are systematic errors introduced by the instrument or the treatment process. They are pretty low, around 3%, but can increase for low or high energies (Fig. 1.2). The second source is the statistical errors, proportional to the square root of counts. This property will make them decrease when the acquisition time will increase. They are dominant at high energy (above 50 GeV) where events are rare. On contrary at low energies (around 100 MeV), the systematic errors dominate. The final equation is the following :

$$\sigma_{tot} = \sqrt{\sigma_{sys}^2 + \sigma_{stat}^2} = \sqrt{\sigma_{sys}^2 + \frac{1}{N}} \quad (1.1)$$

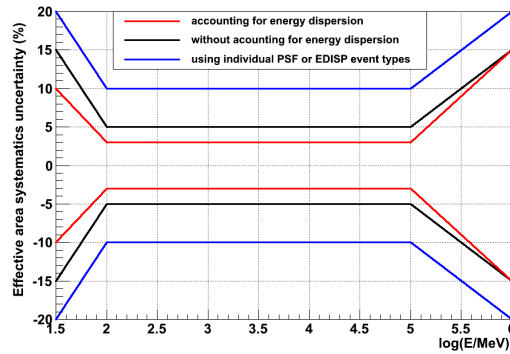


Figure 1.2.: Systematic error for Pass 8 data as function of the energy and the treatment quality. The energy dispersion is an effect of the uncertainty when measuring a photon's energy. Accounting for it when calculating the instrument response function can be critical at very low energies (around a few hundred MeV), where the statistical uncertainties are not dominant anymore.

1.2. Model components

1.2.1. Basic components

1.2.1.1. π^0 production by propagated cosmic rays (PCR)

The initial propagated proton spectrum for the PCR template is obtained from the observed proton data from AMS-02. A good approximation is an unbroken power law ($R-\alpha$) with a spectral index (α) of 2.85 at rigidities above 45 GV. At lower rigidities the data are below the power law because of solar modulation, as seen in Fig. 1.3a, where the AMS-02 data are plotted as well. To find the best parametrization, several indexes and breaks were tested. The optimal parametrization was found by interpolation between the fits with the best test statistic. Finally, the gamma-ray data are well described by an unbroken power law for the protons with a spectral index (α) of 2.85 at all rigidities.

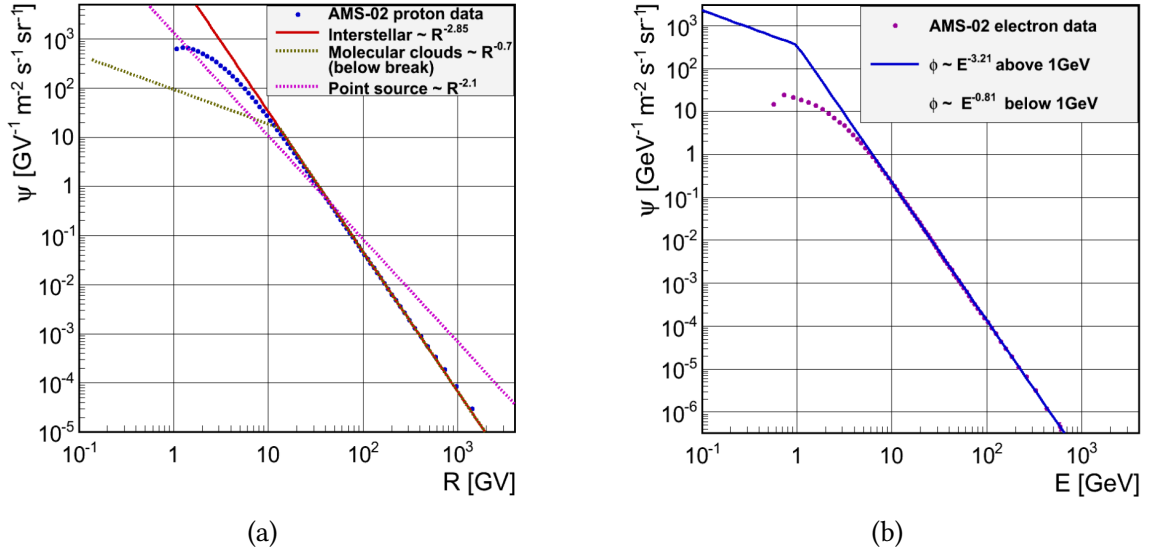


Figure 1.3.: Cosmic ray spectra used to determine the gamma ray templates. (a): Power-law proton spectra used to produce the PCR, MCR and SRC templates. In comparison, the measured data by AMS-02. (b): Power-law electron spectra used to produce the IC and BR templates, compared once again with AMS-02 data.

1.2.1.2. Inverse Compton (IC) and bremsstrahlung (BR)

The interstellar electron spectra needs a break around 0.2 GeV with a spectral index of 3.21 above. This is compatible with the locally observed electron spectrum (see Fig. 1.3b). Below the break the optimal spectral index is 0.81, which implies a suppression of electrons. The targets for the production of gamma-rays are the interstellar gas and the interstellar radiation field (IRF), which are both strongly dependent of position, so the photon composition varies with sky direction. For this reason, we have to calculate the IC templates for each sky direction. The variation over the sky is about $\pm 10\%$, as shown in 1.4a. The BR template only depends on the interstellar gas distribution, decreasing the variations considerably compared to IC, as shown in 1.4b.

1.2.2. Additional components

1.2.2.1. π^0 production by source cosmic rays (SCR)

The proton spectra producing the SCR template can be described by an unbroken power law with a spectral index of 2.1, as obtained from the best gamma-ray template fit. The index 2.1 for the SCR template is expected from diffuse shock wave acceleration. The source cosmic rays are accelerated, or do not have the time to decelerate, hence a harder spectrum at high energies.

1.2.2.2. π^0 production by molecular clouds cosmic rays (MCR)

A proton spectrum with broken power-law can parametrized the decreasing gamma-ray emissivity from MCs below 2 GeV. The break can vary from 6 to 14 GeV for different clouds according to the fit. Above the break an optimal spectral index of 2.85 was found to be the same as for the PCR spectrum, as expected if the high energy propagated protons are above a certain magnetic cutoff. But below the break, , the optimal spectral

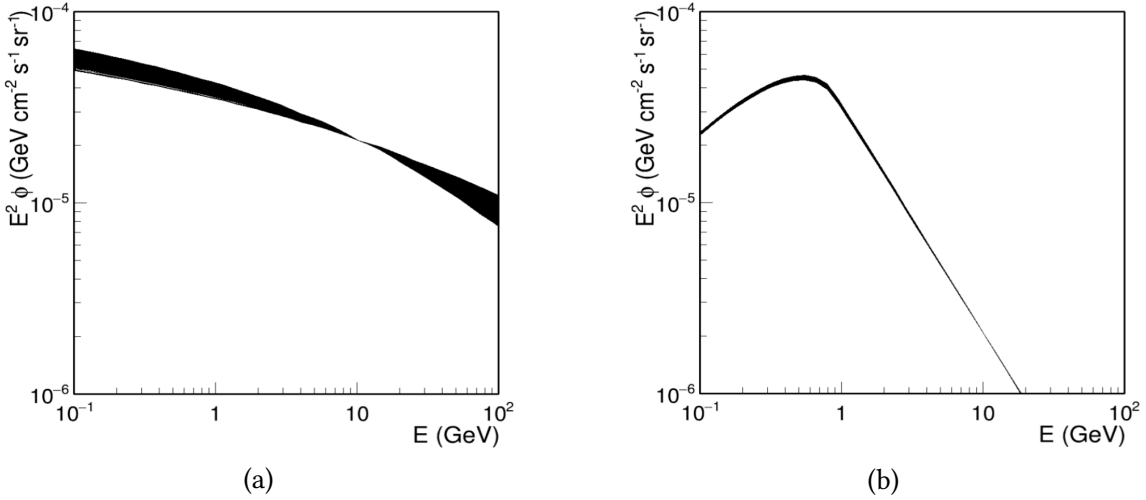


Figure 1.4.: (a): Superposition of the inverse Compton template in every sky direction, normalized at 10GeV. (b): Superposition of the bremsstrahlung template in every sky direction, normalized at 10GeV.

index is 0.7, thus providing a significant suppression of protons below the break, as can be seen from Fig. 1.3a. Variations in the magnetic cutoff in MCs are expected from the variations in size and in magnetic field; the latter increases with MC density. The variations of the break in the proton spectrum between 6 and 14 GeV varies the maximum of the gamma-ray spectrum around a few GeV. The fit prefers a constant spectral index below the break for all sky directions. Such a constant spectral index is plausible with regular magnetic fields oriented in the disk and the "cloudlets" inside MCs form magnetic dipole fields. Then the largest cutoff occurs for cosmic rays entering from the halo perpendicular into the cloud for any orientation of the magnetic dipole. For a given entrance angle the cutoff would provide a sharp break, but for an isotropic distribution of entrance angles the break points are smeared. A distribution of break points will provide a slope below the maximum break determined largely by the isotropic distribution of the entrance angles into the disk. Since this distribution is the same for all MCs the slopes below the break will be similar for all MCs, even if the maximum break varies.

1.2.2.3. Dark matter annihilation (DM)

Dark matter particles are expected to annihilate and produce hadrons of roughly twice the WIMP mass, just like in electron-positron annihilation. This should produce copious amounts of gamma-rays from π^0 decays. A smaller fraction of WIMP annihilation can lead to tau lepton pairs, which can lead to π^0 production in the hadronic tau decays. This contribution is expected to be small and is neglected. The DM template can be calculated with the DarkSusy software. An annihilation signal peaking around 2-3 GeV requires a WIMP mass around 50 GeV, as shown in Fig. 1.5a. The DM template falls down to zero for energies above twice the WIMP mass, which differentiate it from the MCR spectrum with a much softer spectrum.

1.2.2.4. Milli-second pulsars gamma-ray production (MSP)

The MSP template is directly taken from the Fermi study. They simulated the emission of 1700 milli-second pulsars with different energies around the galactic center. The high

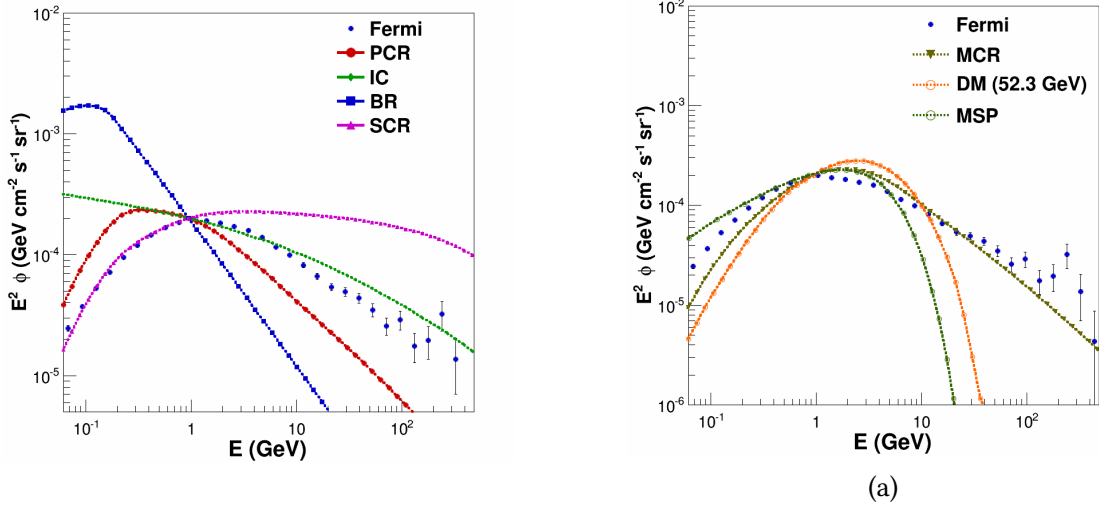


Figure 1.5.: (a): Comparison of PCR, IC, BR and SCR templates, normalized at 1 GeV. Measured data from the central molecular zone is shown as well. (b): Comparison of the three excess components, along with the data from the CMZ.

energy shape of the spectrum resemble closely the DM template, but the main difference with DM and MCR is for low energies. Indeed, below 1 GeV, the MSP template is a lot softer and this feature makes it discernible from the two others.

1.2.2.5. Isotropic component

The isotropic template represents the contribution from the isotropic extragalactic background and hadron mis-identification. Its spectral shape and absolute normalization are provided within the Fermi software, but it was redetermined for the analysis as follow. A first fit of the data in regions outside the Bubbles and the Galactic disk using the isotropic template from the Fermi software is produced as an initial estimate. If one plots the total observed gamma-ray flux versus the fitted flux in the various cones in a certain energy bin, one expects a linear relation crossing the origin if the isotropic flux is estimated correctly (See Fig. 1.6). However, if the isotropic contribution is either too low or too high, an offset at the origin is introduced in the linear relation. Since the isotropic component is by definition the same for all cones for a given energy, this offset can be subtracted from the Fermi template to improve the fit. Once the offset is determined for each energy bin and subtracted from the original template, the process is repeated until the offset converges to zero.

1.3. Fitting method

The fitted data can be seen as a data cube whose dimension are longitude, latitude and energy. The finest spatial grid is divided in 720×360 cones of $0.5^\circ \times 0.5^\circ$. Every cone contains 30 energy bins. This allows to treat different portions of the sky independently of one another. Since the cones do not have the same solid angle and the statistic in a small binning can be problematic, the grid is more often composed of 797 bins of different sizes, bigger at the poles and smaller near the equator. This allows a better statistic in lower flux regions and where a high spatial resolution is not needed (i.e. at high latitudes). In the same time, the equator and the GC have a lot more counts and can be

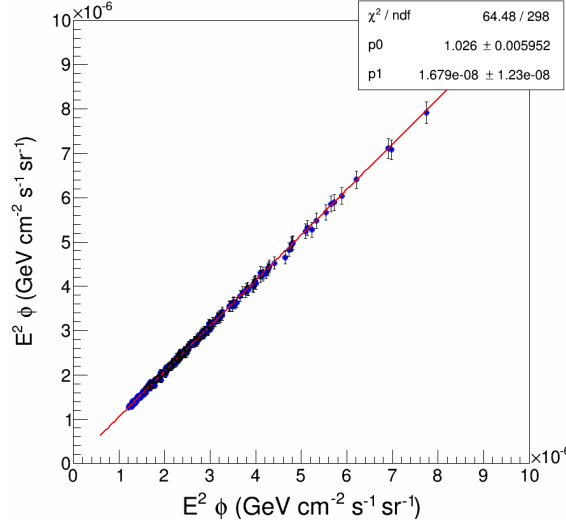


Figure 1.6.: The fitted data (abscissa) versus the observed data (ordinate) in every region of the sky for a given energy of 1 GeV. A linear fit is performed to find the offset at the vertical axis. This number represent the amount the isotropic component shifts the data in all cones. Once this is done for every energy bin, the offset is added to the previous isotropic template and the process is repeated until convergence.

treated in a smaller binning. This binning is way faster to compute than a regular grid with an good enough output quality to study the results.

The fit uses a certain number of components (three at least) each corresponding to a certain phenomenon and described earlier. They all have a certain energy spectra, that can vary with the position in the sky (for PCR, BR and IC). (See Fig. ??

The fits are done for every bin independently. After choosing the templates used for the fit, their scaling factor is the only degree of freedom allowed. Using a ROOT TVirtualFitter object, every template is scaled up or down until their sum comes the closest to the data. Mathematically, the minimum distance between the model and the data is found when the χ^2 value is lowest. It is calculated as follows:

$$\chi^2 = \sum_{i=1}^{30} \left[\frac{(D_i - \sum_{j=1}^n n_j \cdot T_{ij})^2}{\sigma^2} \right] \quad (1.2)$$

where:

- D_i is the data flux in the i^{th} energy bin.
- n_j is the scaling factor for the j^{th} model component.
- T_{ij} is the model flux of the j^{th} in the i^{th} energy bin.
- σ_i is the geometric mean of the statistical and systematical error of the Fermi data point i .

The fit is very well constrained with only five or six degrees of freedoms depending on the model against 30 data points. A useful value is the $\chi^2/d.o.f$ where $d.o.f$ =

$\#data\ points - \#degrees\ of\ freedom - 1$. This rescaling has the advantage to bring the perfect χ^2 value down to one, thus making the comparison between different fits easier. This rescaling will be applied every time when speaking about χ^2 in the rest of the discussion, except if explicitly told. The closest a χ^2 value is to one, the better the model follows the data. The higher it gets, the lower the quality of the fit. It can also happen that it gets lower than one. This can happen when the fit is good, but the error bars on the data are too big.

Since every bin is fitted independently, it is not possible to implement a spatial template, i.e. where the spatial shape of a component would be fixed in advance. For example a component with a spherical distribution around the GC, as can be done in other works. The hope is to let the fit find reasonable shapes by itself only using the χ^2 minimization technique.

This fitting method offers many ways to look at the results, depending on the interest. It is possible to produce flux maps of each component to study their spatial shapes at different energies. This can for example show a correlation between a certain template and a galaxy feature such as the disk or the bubbles. An other way is to create a spectrum of one cone to look at the relative quantity of every template at different energies. This can put into evidence problems in the models and help perfect the spectral shape of the components.

The first step when testing a new model is to see if it can reproduce results of previous studies. Only once it works and can be confidently used can it produce new results.

Bibliography

- [1] Aguilar, M. et al., *Phys. Rev. Lett.* **2013**, *110*, 141102.
- [2] Vagelli, V. Measurement of the cosmic e^+e^- Flux from 0.5 GeV to 1 TeV with the Alpha Magnetic Spectrometer (AMS-02) on the International Space Station. Ph.D. thesis, Karlsruher Institut für Technologie (KIT), 2014.
- [3] BibTeX on Wikipedia, <https://en.wikipedia.org/wiki/BibTeX>, Version Date: 2017-09-19.

List of Figures

1.1.	Measured gamma ray flux before (left) and after (right) point source subtraction in $\text{GeV}/\text{s}/\text{m}^2/\text{sr}$. Most of the spots formed by point sources have disappeared, leaving only the diffuse background emission. The subtraction is not perfect, and can create artificial "holes" in the map (for example at coordinates (90, 25) or (50, 60)).	1
1.2.	Systematic error for Pass 8 data as function of the energy and the treatment quality. The energy dispersion is an effect of the uncertainty when measuring a photon's energy. Accounting for it when calculating the instrument response function can be critical at very low energies (around a few hundred MeV), where the statistical uncertainties are not dominant anymore.	3
1.3.	Cosmic ray spectra used to determine the gamma ray templates. (a): Power-law proton spectra used to produce the PCR, MCR and SRC templates. In comparison, the measured data by AMS-02. (b): Power-law electron spectra used to produce the IC and BR templates, compared once again with AMS-02 data.	4
1.4.	(a): Superposition of the inverse Compton template in every sky direction, normalized at 10GeV. (b): Superposition of the bremsstrahlung template in every sky direction, normalized at 10GeV.	5
1.5.	(a): Comparison of PCR, IC, BR and SCR templates, normalized at 1 GeV. Measured data from the central molecular zone is shown as well. (b): Comparison of the three excess components, along with the data from the CMZ.	6
1.6.	The fitted data (abscissa) versus the observed data (ordinate) in every region of the sky for a given energy of 1 GeV. A linear fit is performed to find the offset at the vertical axis. This number represent the amount the isotropic component shifts the data in all cones. Once this is done for every energy bin, the offset is added to the previous isotropic template and the process is repeated until convergence.	7

Appendix

A. Some appendix section

This appendix chapter contains ...

